IEEE Access
Multidisciplinary | Rapid Review | Open Access Journal

Received June 3, 2019, accepted June 26, 2019, date of publication July 3, 2019, date of current version July 23, 2019.

Digital Object Identifier 10.1109/ACCESS.2019.2926646

Assessment of Blood Vessel Effect on Fat-Intrabody Communication Using Numerical and Ex-Vivo Models at 2.45 GHz

NOOR BADARIAH ASAN[1,2], (Student Member, IEEE), EMADELDEEN HASSAN[3,4], MAURICIO DAVID PEREZ[1], (Member, IEEE), SYAIFUL REDZWAN MOHD SHAH[1], (Student Member, IEEE), JACOB VELANDER[1], TACO J. BLOKHUIS[5], THIEMO VOIGT[6], (Member, IEEE), AND ROBIN AUGUSTINE[1], (Member, IEEE)

[1]Ångström Laboratory, Microwaves in Medical Engineering Group, Solid State Electronics, Department of Engineering Sciences, Uppsala University, SE 751 21 Uppsala, Sweden
[2]Faculty of Electronic and Computer Engineering, Universiti Teknikal Malaysia Melaka, Durian Tunggal 76100, Malaysia
[3]Department of Computing Science, Umeå University, 901 87 Umeå, Sweden
[4]Department of Electronics and Electrical Communications, Menoufia University, Menouf 32952, Egypt
[5]Department of Surgery, Maastricht University Medical Center, 6229 HX Maastricht, The Netherlands
[6]Department of Information Technology, Uppsala University, 752 36 Uppsala, Sweden

Corresponding authors: Noor Badariah Asan (noorbadariah.asan@angstrom.uu.se) and Robin Augustine (robin.augustine@angstrom.uu.se)

This work was supported in part by the Ministry of Higher Education, Malaysia, in part by Eurostars Project under Grant E-9655-COMFORT, in part by the Swedish Vinnova projects for BDAS (2015-04159) and reliable, interoperable and secure communication for body network (2017-03568), in part by the Swedish Foundation for Strategic Research under LifeSec: Don't Hack my Body! project under Grant RIT17-0020, in part by the H2020 EU project SINTEC-824984 (Soft intelligence epidermal communication platform), and in part by eSSENCE (a strategic collaborative eScience program funded by the Swedish Research Council).

ABSTRACT The potential offered by the intra-body communication (IBC) over the past few years has resulted in a spike of interest for the topic, specifically for medical applications. Fat-IBC is subsequently a novel alternative technique that utilizes fat tissue as a communication channel. This work aimed to identify such transmission medium and its performance in varying blood-vessel systems at 2.45 GHz, particularly in the context of the IBC and medical applications. It incorporated three-dimensional (3D) electromagnetic simulations and laboratory investigations that implemented models of blood vessels of varying orientations, sizes, and positions. Such investigations were undertaken by using ex-vivo porcine tissues and three blood-vessel system configurations. These configurations represent extreme cases of real-life scenarios that sufficiently elucidated their principal influence on the transmission. The blood-vessel models consisted of ex-vivo muscle tissues and copper rods. The results showed that the blood vessels crossing the channel vertically contributed to 5.1 dB and 17.1 dB signal losses for muscle and copper rods, respectively, which is the worst-case scenario in the context of fat-channel with perturbance. In contrast, blood vessels aligned-longitudinally in the channel have less effect and yielded 4.5 dB and 4.2 dB signal losses for muscle and copper rods, respectively. Meanwhile, the blood vessels crossing the channel horizontally displayed 3.4 dB and 1.9 dB signal losses for muscle and copper rods, respectively, which were the smallest losses among the configurations. The laboratory investigations were in agreement with the simulations. Thus, this work substantiated the fat-IBC signal transmission variability in the context of varying blood vessel configurations.

INDEX TERMS Blood vessel, channel characterization, fat-IBC, intrabody microwave communication, path loss.

I. INTRODUCTION

Intra-body communication (IBC) can be described as a communicative technique, with the human body serving as the vessel for communication. It effectively connects different types of devices that can be worn and attached on or under the body surface. IBC can be deployed using various methods, such as radio frequency (RF) [1]–[3], galvanic coupling [4]–[7], capacitive coupling [8]–[10], ultrasound [11], [12], and resonant coupling [13]–[15].

The associate editor coordinating the review of this manuscript and approving it for publication was Mahmoud Al Ahmad.

The advancing years have culminated in the novel method of Fat-Intrabody Microwave Communication (Fat-IBC), which is conceptualized in the notion of utilizing fat tissue present between two tissues of high permittivity (i.e. skin and muscle). The transmission medium has been shown to be feasible at and around the microwave frequency of 2.0 GHz in [16], as well as at the R-band frequencies (1.7–2.6 GHz) [17]. Furthermore, [18] has successfully substantiated 96 % of packet reception rate (PRR) at 2.0 GHz using the medium in the setup of phantom-based and ex-vivo porcine tissue-based investigation. Prior to further implementation of the IBC signal, a quantitative assessment of the biological tissue and the subsequent impacts are undeniably crucial. Ensuring the reliability of the fat-IBC medium calls for the fundamental investigation into the attributes for the channel propagation.

Signal transmission and its quality may be influenced by various factors, with different works and publications highlighting the impact of multiple natural bodily effects in IBC. They include: limb joints and movement in capacitive coupling [19], [20], limb gestures on galvanic coupling [21], [22], muscle stress [23], body movement [24], human skin fibroblast cells [25], body mass index [26], and differing fat tissue thicknesses [27]. However, the fat-IBC technique reliability has only been looked into by several works in the context of parameters capable of influencing the channel's performance. Examples of recent investigations include those that affect the transmission channel, such as embedded muscle tissue [28], nonhomogeneous fat tissue thickness [27], and blood vessel [29]. The outcomes of these experiments revealed fat-IBC's capacity for excellent communication even in the presence of up to 60 % obstacles of channel height [28]. The signal transmission was not impacted by obstacle less than 15 mm cube and it starts to degrade when the 25 mm height channel is perturbated with a perturbating tissue of size 15 mm cube and above. Furthermore, a maximum loss of 4 dB/cm has been shown for the fat-IBC in a channel of 5 mm thickness, whereby the signal coupling is found to increase parallel to increasing fat tissue thickness [27].

Generally, fat offers less electric conductivity and dielectric constant relative to its surrounding tissues be it skin or muscle, which subsequently enhances microwave transmission due to its lower attenuation [30]. In contrast, other bodily components of blood, nerves, and muscles among others are characterized with high water content and high losses [30], whereas the fat tissues are packed with many nerve cells and blood vessels [31]. A preliminary blood vessel study regarding its influence upon communication has been undertaken previously using numerical modeling [29]. Therefore, this work is aiming to undergo a comprehensive assessment regarding the influence of blood vessel signal transmission upon fat-IBC.

This work opted to incorporate three different positions for blood vessels in fat tissue, which were categorized according to their orientations relative to the tissue. Simulation was conducted by using the Computer Simulation Technology (CST) microwave studio software (https://www.cst.com/), while model validation was undertaken by performing ex-vivo porcine tissue measurement. The measurement indicated the simulation outcomes upon blood vessel embedment into fat tissue. Then, the measurements were utilized for the transmission coefficient analysis for all three planes using factors such as blood vessel diameter, number of blood vessels, and relative position of blood vessel from the transmitter. Result extraction was conducted using data sweep at the frequency of 2.45 GHz, while signal transmission of the configurations was compared using a 100 mm length reference channel lacking blood vessels. Besides, each of the electric field distribution was analyzed for the purpose of comprehending microwave dissemination on fat channel.

This work is structured according to the follow flow accordingly. First, Section II explains the fat-IBC technique, followed by Section III that describes the three configurations based on blood vessel tissue arrangements and directions in the fat tissue. The configuration modeling has been carried out in the longitudinal, transverse-vertical, and transverse-horizontal planes relative to the microwave propagation, whereby further explanation regarding their respective measurement setup has been provided. Then, results obtained from the simulation and measurements have been depicted accordingly, with a discourse on the impacts of blood vessels towards fat-IBC (including electric field) is included in Section IV. Lastly, Section V outlines the conclusion as a result of this work.

II. FAT-INTRA BODY COMMUNICATION (Fat-IBC)

Fat-IBC is a novel technique incorporating fat tissue as the communication medium between implanted devices. Figure 1 depicts the tissue and its three layers of skin, fat, and muscle for the technique. Following microwave signal propagation throughout the fat tissue, the signal coupling through the tissue was investigated. The setup served as a reference in assessing the influence of signal coupling with the presence of blood vessels in the fat tissue in the subsequent section.

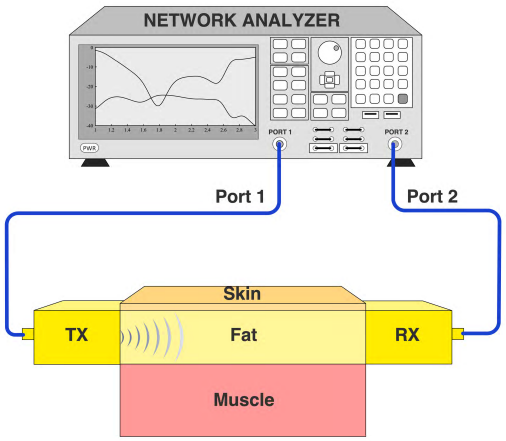

FIGURE 1. Microwave propagation through the fat layer in three-layered homogeneous skin, fat, and muscle.

TABLE 1. The dielectric properties of the ex-vivo tissue and other materials used in the experimental setup at 2.45 GHz frequency.

Tissue / Material	Ex-vivo tissue / Measured		Human tissue / Database [35]	
	Permittivity	Conductivity (S/m)	Permittivity	Conductivity (S/m)
Skin	40 ± 4	1.4 ± 0.1	38 ± 2	1.5 ± 0.1
Fat	5.5 ± 0.5	0.12 ± 0.01	5.3 ± 0.3	0.1 ± 0.01
Muscle	51 ± 5	2.2 ± 0.2	53 ± 3	1.7 ± 0.1
Blood vessel	N/A	N/A	43 ± 2	1.4 ± 0.1
Copper rod	N/A	5.96×10^7	N/A	N/A
Polylactic Acid (PLA) plastic	2.6 ± 0.3	0.12 ± 0.01	N/A	N/A

III. MATERIALS AND MEASUREMENT SETUP

This study incorporated the three factors of sizes, positions, and number of blood vessels during the assessment. Berne and Levy Physiology [32] have described that there are five primary groups of blood vessel, such as arteries, arterioles, capillaries, venules, and veins. Based on this, Asan *et al*. [29] have opted to evaluate the impact of all three kinds of blood vessels on signal coupling, namely arterioles, arteries, and veins. The mean diameters of the blood vessels are 30 μm, 4 mm, and 5 mm, respectively. With regard to the outcomes yielded, the arterioles did not reveal a significant decrement of signal coupling compared to the reference, which lacked blood vessels.

This work utilized the muscle tissue and copper rods to emulate blood vessel models, whereby their selection was due to similarities in dielectric attributes and high conductivity, respectively. The copper rod had higher conductivity compared to blood vessels, rendering the outcomes estimating worst-case scenarios of blood vessels with extreme materials contrast relative to the fat channel. Table 1 depicts the dielectric attributes of each tissue and materials utilized when measuring them.

To measure the ex-vivo tissue, we used the slim probe in the Keysight N1501A Dielectric Probe Kit, which has, according to datasheet, a typical uncertainty of 10 % (refer page 6 in [33]). Because the statistical variation (Type A uncertainty) of these measurements was found to be much lower than the datasheet uncertainty (Type B uncertainty), we simplified the uncertainty reporting as 10 % of the value as displayed in Table 1. For the human tissue, we used the database by Italian National Research Council (http://niremf.ifac.cnr.it/tissprop/) which is based in the work of Gabriel *et al*. [34], [35] and has been improved in the modeling. The reported uncertainty for the database which, is not stated was based in [36] and is similar to ours, even though in some cases lower.

Because the measurement of biological tissues is a challenging task and there are many factors that could influence the measurement, we believe that an uncertainty between 5 to 15 % is normal and could help to guide the research, but effort should be put to reduce the uncertainty of the measurement. We can see that our ex-vivo measurement and the database are comparatively similar and that the reported values between different tissues are well distinguishable.

The manual insertion of blood vessel models was undertaken using the three configurations of the transverse-vertical, transverse-horizontal, and longitudinal planes for signal propagation across the fat tissue. They were the representative configurations for different blood vessel orientations that may possible happen in the fat channel. Signal coupling measurement using these configurations would elucidate the influence of blood vessels upon the transmission channel. The transverse-vertical and transverse-horizontal planes were characterized with blood vessels positioned at 10, 30, 50, 70, and 90 mm from the transmitter (TX), while the measurements were taken at each blood vessel location and diameters. Meanwhile, Figure 2 reveals the position of the blood vessel in the fat tissue, whereby simplified illustration included depicts fat layer in the different planes accordingly (Figure 2a: Longitudinal; Figure 2b: Transverse-vertical; and Figure 2c: Transverse-horizontal). The fat layer was wedged between the top layer of skin of 2 mm thickness according

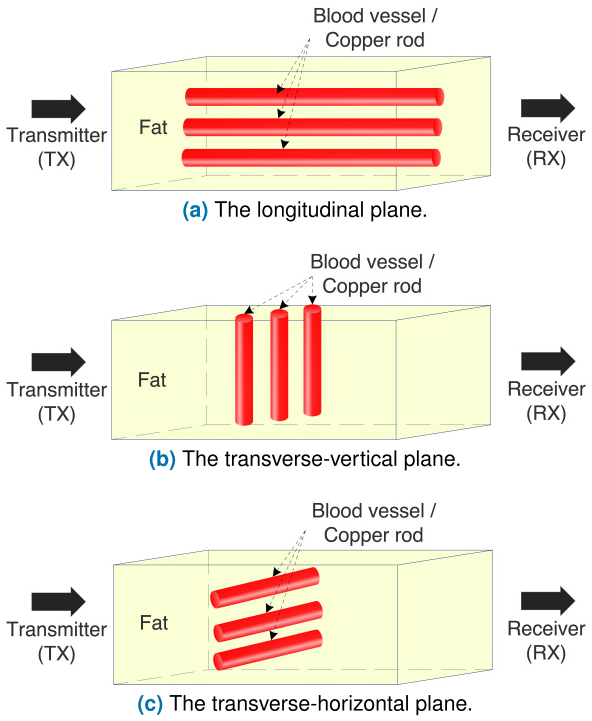

FIGURE 2. Simplified diagram of blood vessel orientations in the fat layer.

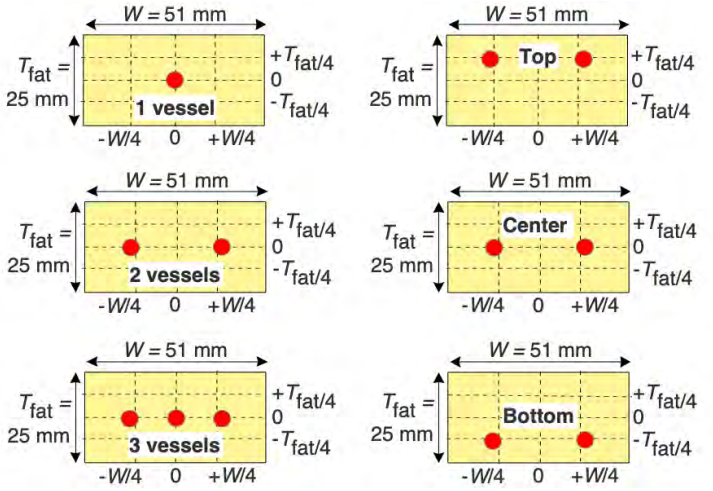

(a) The longitudinal plane. The cross-section view through the fat channel showing blood vessels as red dots.

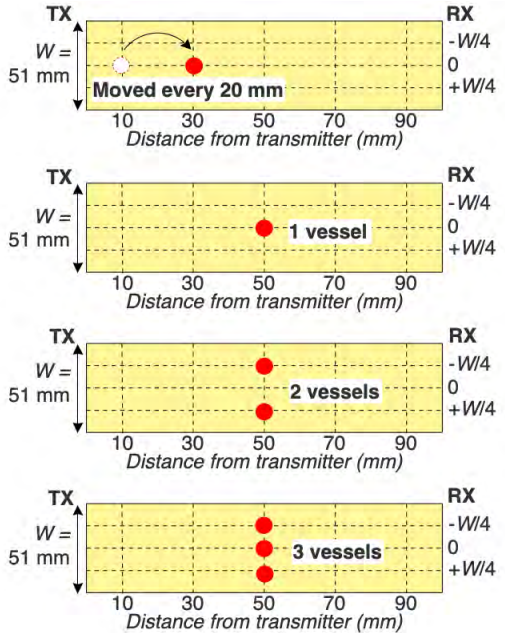

(b) The transverse-vertical plane. The longitudinal-horizontal section view showing blood vessels as red dots.

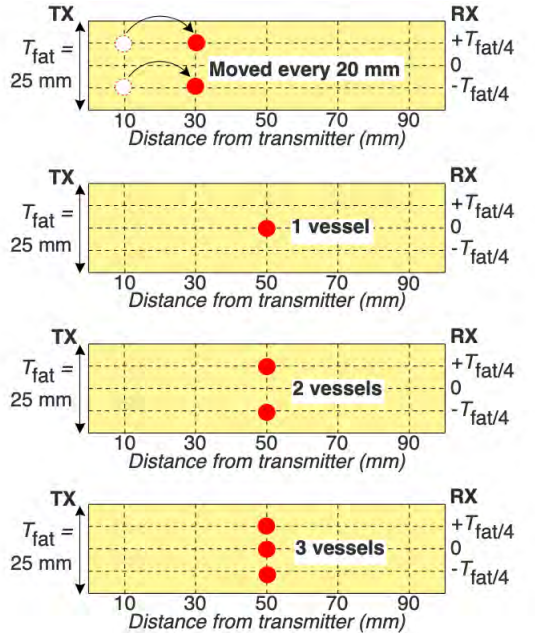

(c) The transverse-horizontal plane. The longitudinal-vertical section view showing blood vessels as red dots.

FIGURE 3. **The positions of the blood vessel model in the fat tissue layer.**

to typical values [37] and bottom layer of muscle, which was 30 mm in thickness. The stark difference of muscle layer thickness was attributable to its minimal impact signal transmission [16].

Figure 3 depicts the varying locations and dimensions of the blood vessel model in the fat tissue, whereby Figure 3a reveals the side-view according to the TX side. Meanwhile, the three images shown at the left side show the position at which the number of vessel multiply from one vessel to three. Such position is calculated via division by $^{-W}/_{4}$, 0 (center), and $^{+W}/_{4}$, where W is the sample width, $^{-W}/_{4}$ is situated to the left of the width, and $^{+W}/_{4}$ is situated to the right of the width. In contrast, the three images shown at the right side show the position at which the blood vessel insertion occurs at the top, center, and bottom of the fat tissue. This is allocated as $+T_{\mathrm{fat}/4}$, 0 (center), and $-T_{\mathrm{fat}/4}$, where T_{fat} is the fat tissue thickness, $+T_{\mathrm{fat}/4}$ is the blood vessel placement close to the layer of skin, and $-T_{\mathrm{fat}/4}$ is adjacent to layer of muscle. Next, Figure 3b depicts the vessel location from the upper view of the transmission, which is calculated via division by $^{-W}/_{4}$, 0 (center), and $^{+W}/_{4}$ across the thickness of the fat tissue. Meanwhile, Figure 3c depicts the blood vessel location from

the frontal view of the transmission channel, whereby the vessels are located at $+T_{\text{fat}/4}$, 0 (center), and $-T_{\text{fat}/4}$ across the width of the channel. Both configurations implemented vessel movement from 10 mm to 90 mm by 20 mm step (see Figures 3b and 3c).

A comprehensive experiment was set up to assess the effect of blood vessel upon the fat-IBC as shown in Figure 4. It consisted of the following: a Fieldfox Microwave Analyser [38], a pair of rectangular waveguide probes [17], [39], a three-layered ex-vivo porcine tissue comprised of skin, fat, and muscle (top to bottom), and blood vessel models with three different diameters.

A mold container of dimension 61 mm $\times$ 230 mm $\times$ 63 mm ($w \times l \times h$) was produced using a 3D printer with polylactic acid (PLA) plastic filament, which possessed the dielectric attribute of 2.6 ± 0.3. Ex-vivo porcine tissue consisting of skin, fat, and muscle was placed into the plastic container, having the thickness of 2 mm, 25 mm, and 30 mm, respectively, and stacked from top to bottom. The fat and muscle were sourced from newly-slaughtered porcine belly of the local slaughterhouse, which was separated and minced finely using meat mincer. This work opted for a total distance of transmission of 100 mm between the transmitter and receiver. Difficulties in obtaining the copper rods necessary having the precisely identical size as the actual blood vessel in markets resulted in the use of three copper rod of various sizes. Their respective sizes were comparable to human blood vessel to fully comprehend their effect towards signal coupling. Meanwhile, molds shaped as cylinder tubes with diameters of 2 mm, 4 mm, and 6 mm diameter sizes each and 0.4 mm wall thickness were produced using 3D printing to be loaded in the muscle tissue. Such configurations were obtained using blood vessel diameter size of 2 mm, 4 mm, and 6 mm diameter rod. Then, the microwave analyzer was utilized to undertake the ex-vivo measurement using differently-sized rod sizes and positions in the fat tissue in order to assess their effect on the transmission coefficient, S_{21} within 1 GHz to 4 GHz frequency range. All assessments were carried out at room temperature (22 °C) and a pair of waveguide probes was implemented to assess the influence of blood vessel dimension and position. This was achieved by its role of supplying and receiving the microwave signal across the fat tissue.

In Figure 4, the experimental setup of three varying configurations are depicted accordingly. Figure 4a reveals the setup across the longitudinal plane throughout the propagation direction, where Probe 1 was connected to port 1 of the Microwave Analyser and functioned as the transmitter. Meanwhile, Probe 2 was connected to port 2 and functioned as the receiver. Next, Figure 4b reveals the transverse alignment for the blood vessel models across the transmission line, whereby porcine skin was on top of the fat and the minced muscle tissue was at the bottom. This resulted in the boundary confinement of the fat-IBC. Then, the 3D mold container was used to produce a longitudinal window having a printed centimeter scale, which allowed blood vessel model insertion in

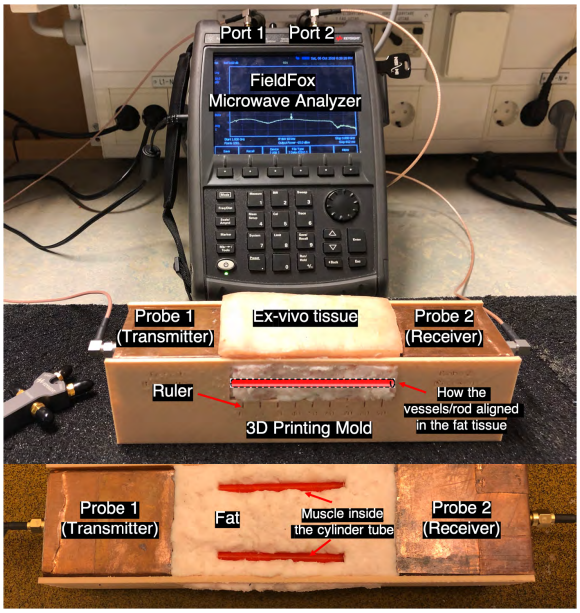

(a) The longitudinal plane.

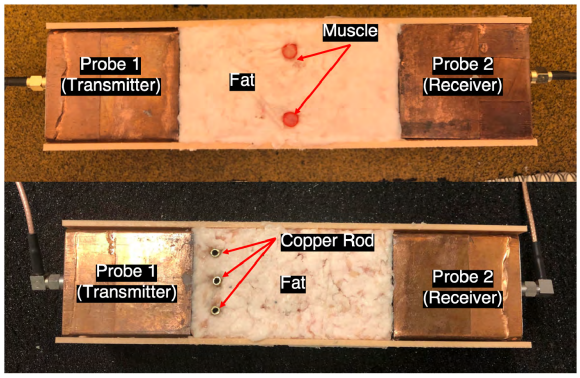

(b) The transverse-vertical plane.

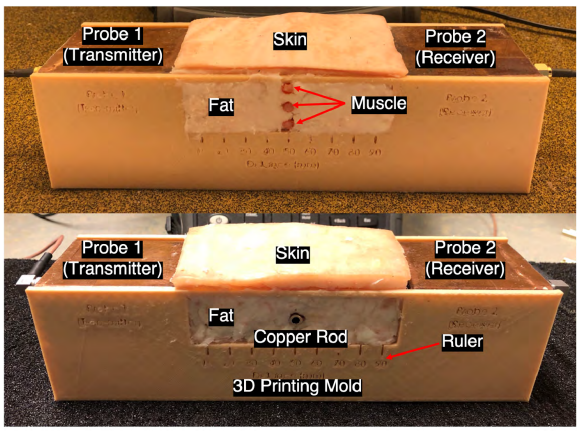

(c) The transverse-horizontal plane.

FIGURE 4. Experimental setup.

the transverse-vertical and transverse-horizontal plane positions. Such step was taken to minimize observational error that occurred during measurement, while a reference measurement was recorded prior to blood vessel model insertion

for all configurations (muscle or copper rods). In Figure 4c, the setup depicting 90° rotatory position of the blood vessel models in the transverse plane (Transverse-horizontal). The rods were subjected to displacement from 10 mm to 90 mm of distance away from the transmitter in 20 mm steps, whereas the amount of blood vessel models were multiplied from one to three rods.

IV. RESULTS AND DISCUSSION

This study expressly emphasized the impact of different blood vessel model configurations produced using muscle tissue and copper on the transmission channel. Therefore, the magnitude of the transmission coefficient, S_{21} in each case is assessed accordingly as seen in Figure 2, with the fat channel that lacked the blood vessel models. Figures 5, 6, 10, 11, 14, and 15 each depict red solid lines to represent the S_{21} measurement and simulation outcomes for the signal transmission at 100 mm distance. They also functioned as the reference line in assessing the effect of blood vessel in the channel towards signal coupling, which yielded –26.81 dB (measurement) and –27.39 dB (simulation), respectively, for the fat channel (red reference line). The resulting transmission coefficient recorded due to the measurement was presented alongside the simulation outcomes.

Figure 5 and 6 each depict the simulated and measured S_{21} values for longitudinal plane according to muscle and for copper rod configurations, respectively. Figure 5 clearly shown that the magnitude of S_{21} decreased alongside the incremental amount of muscle rods in the fat tissue (i.e. from one to three rods). Furthermore, muscle rods of 2 mm and 4 mm diameters revealed lesser effect towards signal coupling compared to its 6 mm diameter counterpart, which was proportional to the simulated values. In contrast, the 6 mm diameter yielded increased signal coupling alongside incremental number of rods by ∼0.2–1.6 dB for both simulated value and actual measurement. Therefore, particular configuration produced dissimilar trends in case of copper rods being present. In Figure 6, higher signal coupling effect is seen upon copper rod placement within the fat at $+T_{\text{fat/4}}$ below the skin in comparison with its placement at $-T_{\text{fat/4}}$ on top of the muscle. The significant decrement of signal coupling at position $+T_{\text{fat/4}}$ below skin was attributable to the difference in permittivities between the skin and muscle. As the skin was thinner and had lesser permittivity compared to the muscle, discontinuities were generated in the signal coupling. Similarly, it may also be explained by the copper rod positioning, which hindered some of the signal transmission across the fat tissue.

In Figure 7, the electric field (E-field) is conjured up at 2.45 GHz for the fat channel with the lack of blood vessel to function as the reference. The E-field can be seen to be propagated throughout the tissue, remains limited between the layers of skin and muscle.

Next, the longitudinal plane cases were assessed using a rod of 60 mm long, which was placed in the middle of the transmission channel to prevent a strong interaction between

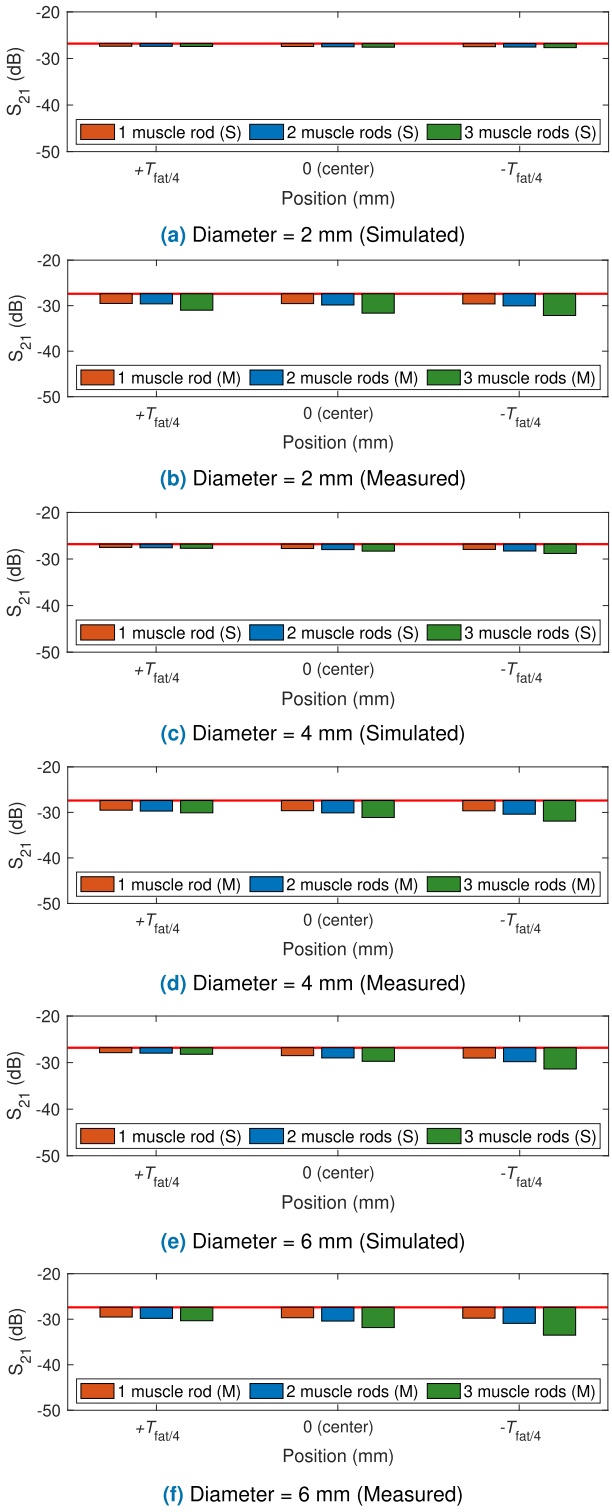

FIGURE 5. MUSCLE ROD: Simulated and measured S_{21} results for longitudinal plane with 60 mm length rods. (a, b) Diameter = 2 mm. (c, d) Diameter = 4 mm. (e, f) Diameter = 6 mm.

the probes and blood vessels. All outcomes subjected to simulations using three muscle tissues so as to emulate the blood vessel for all scenarios using the 2 mm and 6 mm diameter rods. This allowed the projection of a worst-case scenario

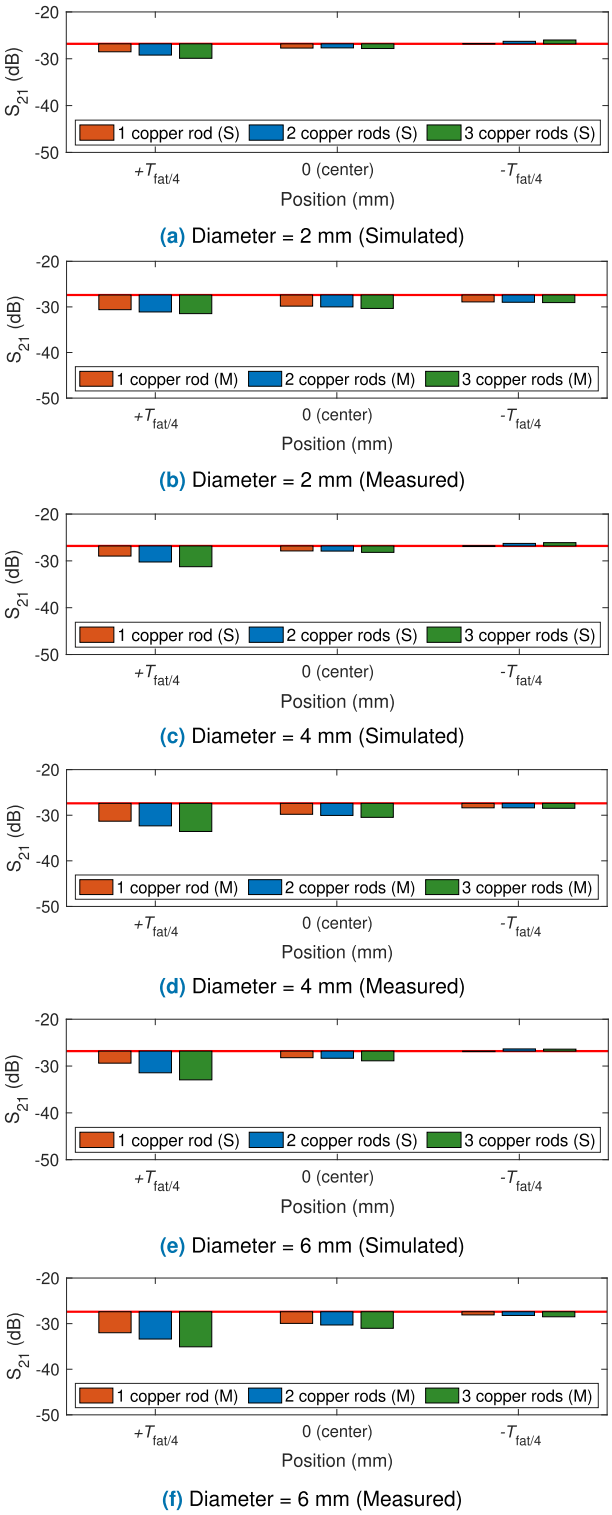

FIGURE 6. COPPER ROD: Simulated and measured S_{21} results for longitudinal plane with 60 mm length rods. (a, b) Diameter = 2 mm. (c, d) Diameter = 4 mm. (e, f) Diameter = 6 mm.

and assessment of the correlation between the E-field pattern and the signal coupling, S_{21} in this work. Figure 8 depicts the lesser impacting outcome for E-field due to the blood vessels (see Figures 8a, 8b, and 8c), whereby Figure 8d reveals that the E-field is displayed when the 6 mm diameter blood vessels

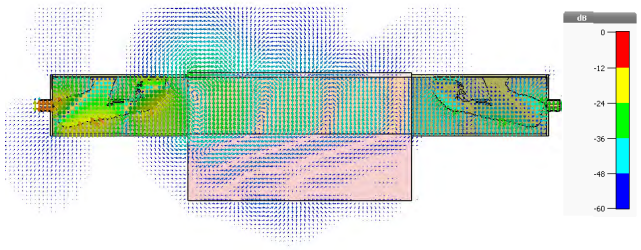

FIGURE 7. Electric field for the fat channel (Reference) with scalar mapping in decibel (dB).

are aligned near to the muscle. Meanwhile, Figure 9 shows that the E-field shift when the copper rods are adjacent to the skin $+T_{\text{fat/4}}$ (see Figure 9a and 9c). Blockage present in the channel minimized the channel thickness and impacted signal couple due to varying E-field in the waveguide that propagated in the transverse electric mode. A signal transmission displays shifting and attenuation in a channel if a conductive material is situated alongside the propagation direction. Therefore, the larger blood vessels in the channel is obviously more impactful compared to their smaller counterparts.

In Figures 10 and 11, further analysis of the blood vessel impact on the fat tissue is performed by positioning the blood vessel models vertically along the fat tissue. They depicted the impact of signal coupling in the transverse-vertical plane across varying locations for different rod sizes accordingly. Both figures show decreasing S_{21} as the number of rods multiply from one to three, while muscle rods of Figure 10 depict lesser effect compared to the copper rods of Figure 11. In case of the muscle tissue at the maximum diameter size and maximum number of vessels, the signal coupling was decreased by 5.13 dB (measurement) and 5.11 dB (simulation) relative to the reference channel as seen in Figures 10e and 10f. Meanwhile, the copper rods revealed a significant reduction of signal coupling up to 17.13 dB (measurement) and 14.31 dB (simulation) as depicted in Figures 11e and 11f. Such notable loss of energy is explainable by the high level of reflection due to copper rods, which are characterized with high conductivity. If these rods are positioned vertically relative to the transmitter, the electric field will display orthogonal propagation towards the transmission direction as they function as the reflector in the fat channel. This also rendered them to be considered as the transmission line. Stark transverse electric field discontinuity in the transmission channel will significantly disturb the signal propagation, causing substantial signal loss. Moreover, increased copper rod size causes a bigger obstacle within the propagating path, rendering the signal reflected back to generate increased energy loss. In contrast, muscle tissue is characterized with comparable dielectric attributes as the blood vessel and remains less impacted to yield less reflection. However, varying signal coupling may be seen due to blood vessel diameter changes, as dissimilar distances and factors have resulted in comparable trends between the simulation and measurement outcomes.

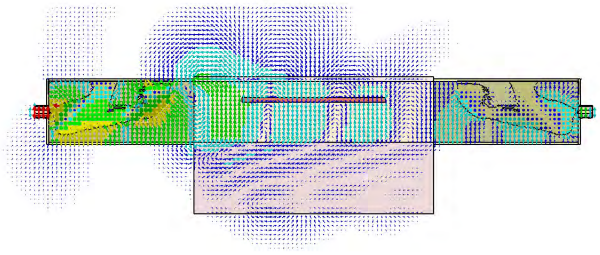

(a) Three 2 mm diameter vessels aligned at $+T_{\text{fat/4}}$ below the skin.

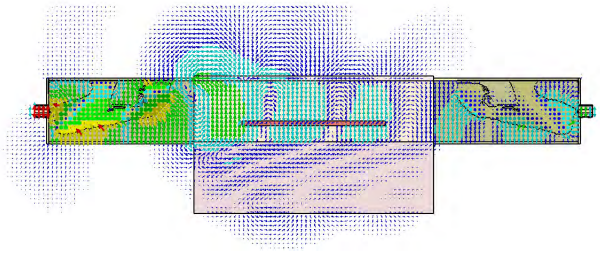

(b) Three 2 mm diameter vessels aligned at $-T_{\text{fat/4}}$ on top of the muscle.

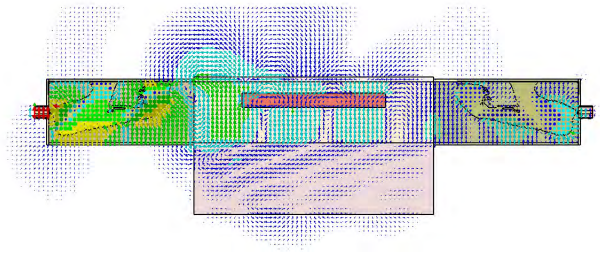

(c) Three 6 mm diameter vessels aligned at $+T_{\text{fat/4}}$ below the skin.

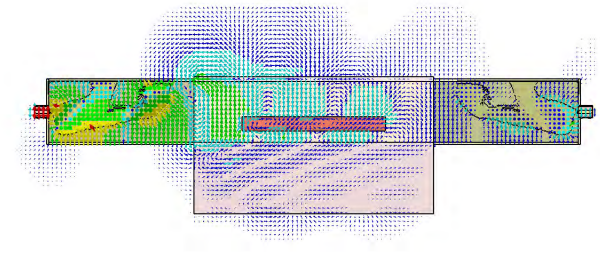

(d) Three 6 mm diameter vessels aligned at $-T_{\text{fat/4}}$ on top of the muscle.

FIGURE 8. MUSCLE ROD: Electric field for three blood vessels in longitudinal plane.

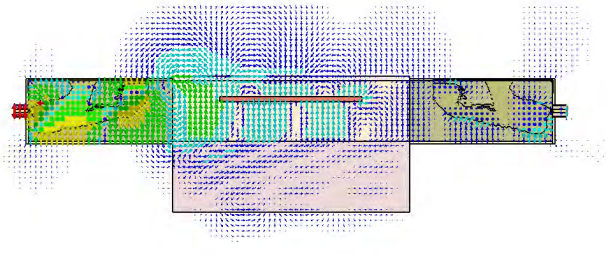

(a) Three 2 mm diameter vessels aligned at $+T_{\text{fat/4}}$ below the skin.

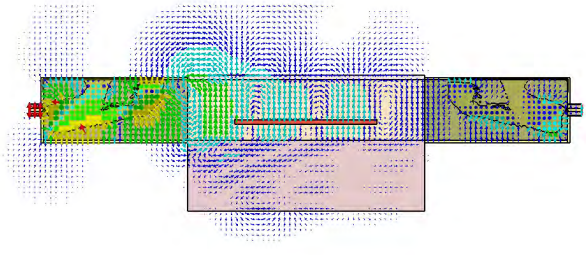

(b) Three 2 mm diameter vessels aligned at $-T_{\text{fat/4}}$ on top of the muscle.

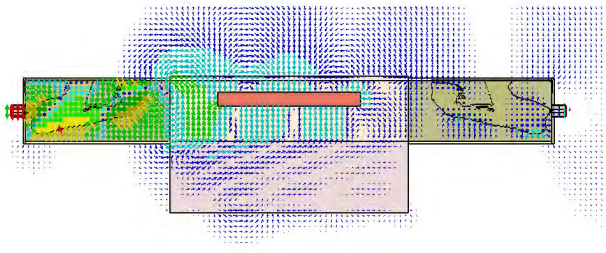

(c) Three 6 mm diameter vessels aligned at $+T_{\text{fat/4}}$ below the skin.

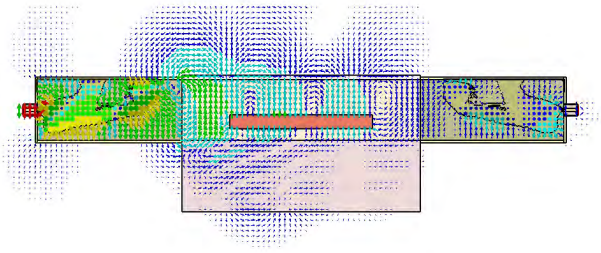

(d) Three 6 mm diameter vessels aligned at $-T_{\text{fat/4}}$ on top of the muscle.

FIGURE 9. COPPER ROD: Electric field for three blood vessels in longitudinal plane.

Visualization of the dissimilar signal coupling occurrences with the blood vessel being present in the transverse-vertical configurations is achievable due to E-fields being depicted for both muscle and copper rods. In Figures 12 and 13, the E-field is shown as blood vessels align accordingly in the transverse-vertical plane. Muscle tissue found in the fat resulted in the continuous propagation of the E-field, as seen in Figures 12a and 12b. In contrast, Figures 13a and 13b depict discontinuous propagation of the E-field distribution and significant decrement of the signal coupling. This is due to the copper rods, which caused the electromagnetic wave to impinge on a conductive material and the E-field to be reflected by the conductor [40].

In Figures 14 and 15, the simulated and measured S_{21} values for the transverse-horizontal plane cases are shown accordingly. The outcomes obtained for S_{21} as a function of positions and numbers of muscle and copper rods are also displayed in the figures. From the simulation carried out, the S_{21} magnitude decreased gradually parallel to the increasing number of blood vessel from one to three rods.

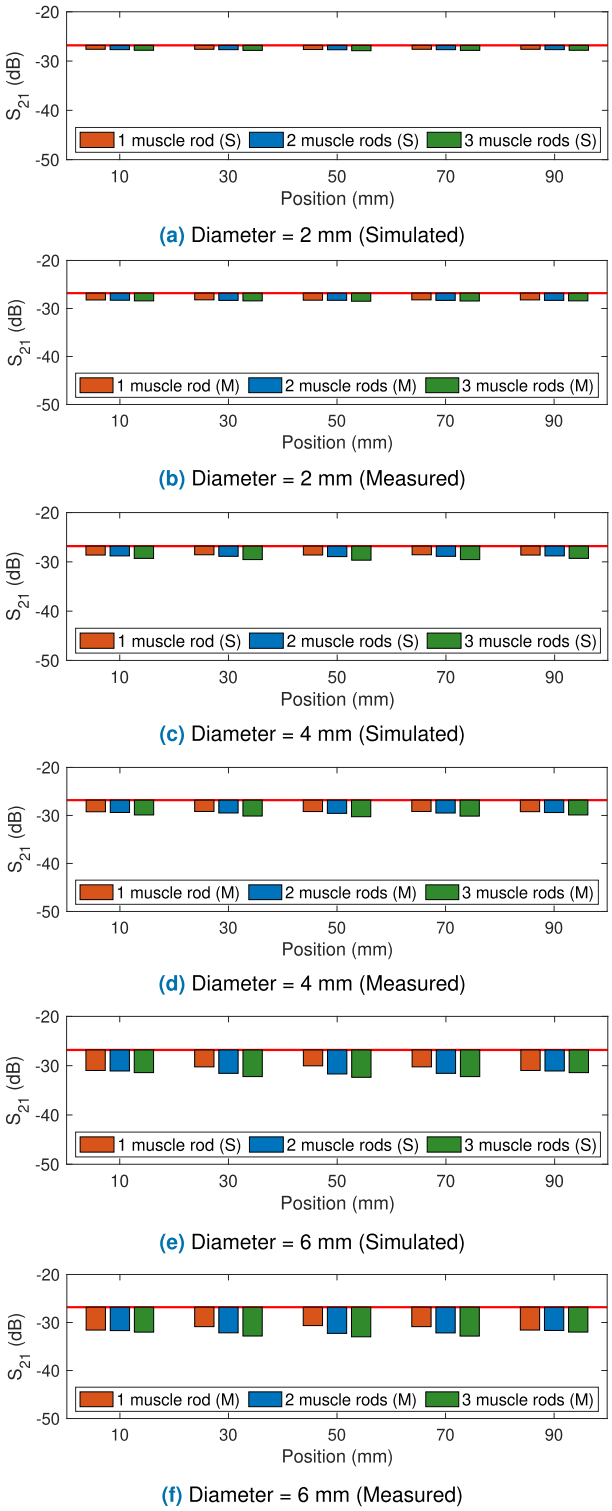

FIGURE 10. MUSCLE ROD: Simulated and measured S_{21} results for transverse-vertical plane. (a) & (b) Diameter = 2 mm. (c) & (d) Diameter = 4 mm. (e) & (f) Diameter = 6 mm.

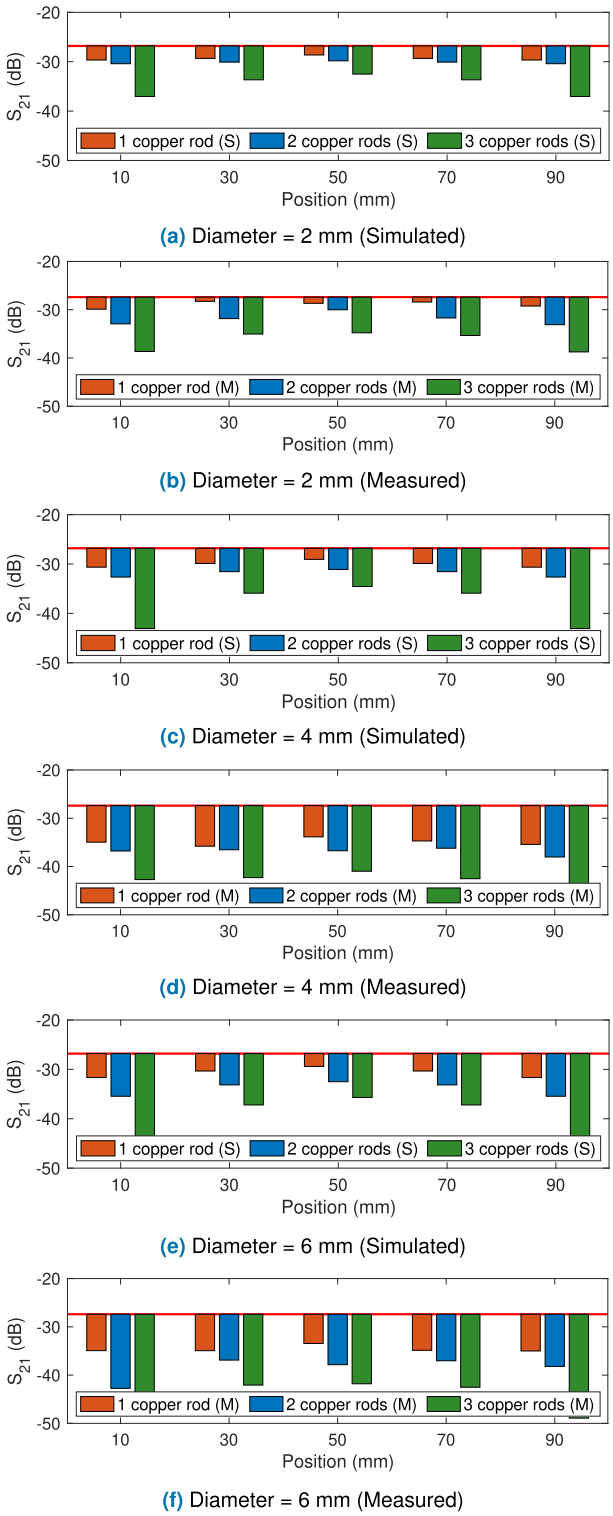

FIGURE 11. COPPER ROD: Simulated and measured S_{21} results for transverse-vertical plane. (a) & (b) Diameter = 2 mm. (c) & (d) Diameter = 4 mm. (e) & (f) Diameter = 6 mm.

Therefore, blood vessel and its presence is less effective in impacting the signal coupling of a transmission relative to the fat channel. Such occurrence can be explained by the discontinuous propagation caused by the waveguide in case of transverse-horizontal placement of the blood vessels. This results in it functioning as the splitter and recombiner, rendering the electromagnetic signal to be divided and then recombined. As of present, the differences depicted were

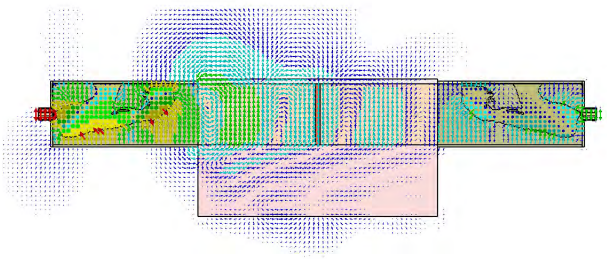

(a) Three 2 mm diameter vessels aligned at 50 mm distance from transmitter.

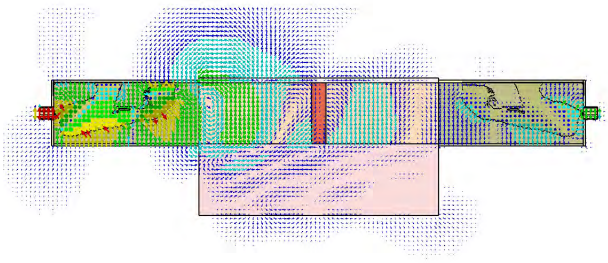

(b) Three 6 mm diameter vessels aligned at 50 mm distance from transmitter.

FIGURE 12. MUSCLE ROD: Electric field for three blood vessels in transverse-vertical plane.

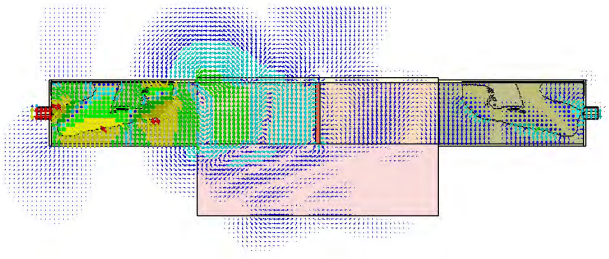

(a) Three 2 mm diameter vessels aligned at 50 mm distance from transmitter.

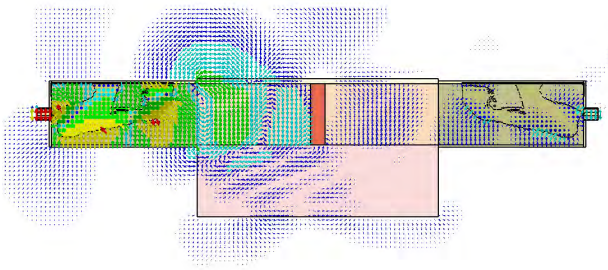

(b) Three 6 mm diameter vessels aligned at 50 mm distance from transmitter.

FIGURE 13. COPPER ROD: Electric field for three blood vessels in transverse-vertical plane.

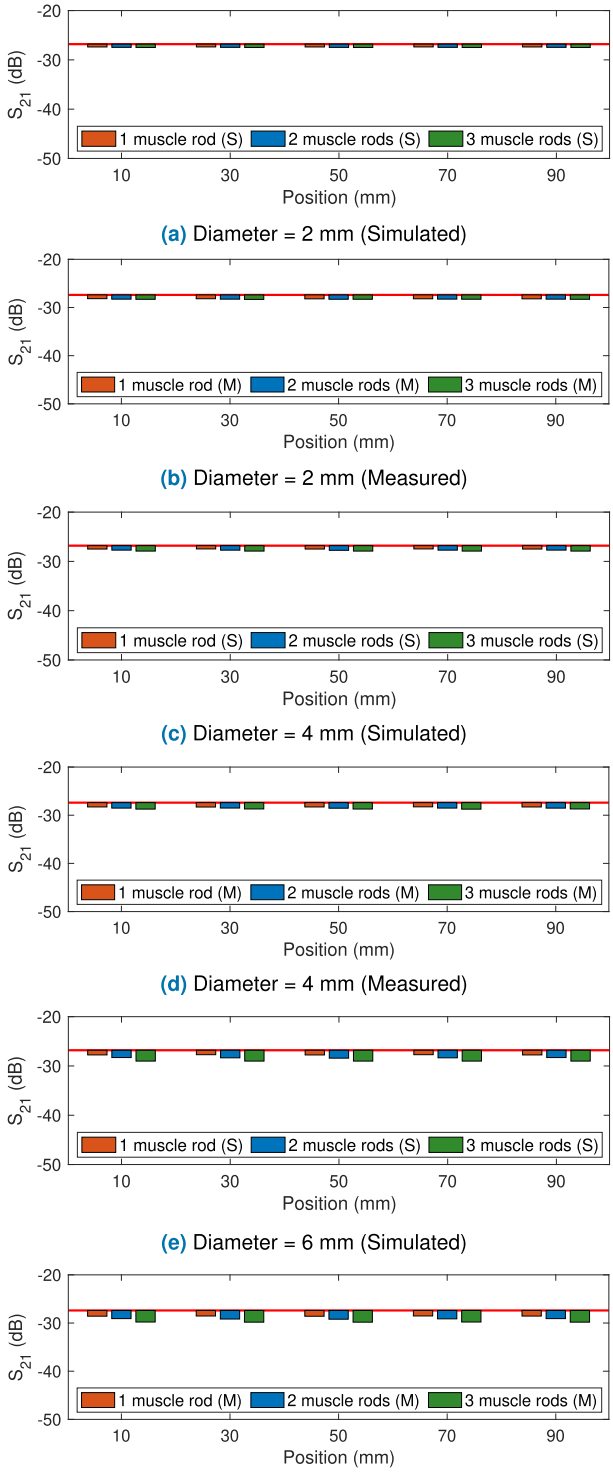

FIGURE 14. MUSCLE ROD: Simulated and measured S_{21} results for transverse-horizontal plane. (a, b) Diameter = 2 mm. (c, d) Diameter = 4 mm. (e, f) Diameter = 6 mm.

correlated to the misaligned copper rod placement during the measurement, which was further shown per the stark discrepancy between the values obtained in the experiment versus those yielded by dissimilar value of dielectric attribute of the ex-vivo tissue. This was apparent across the entire experiment relative to the values imported from the simulation. The transverse-horizontal aligned rods as seen in Figure 16 reveals less attenuation effect for the E-Field in the channel

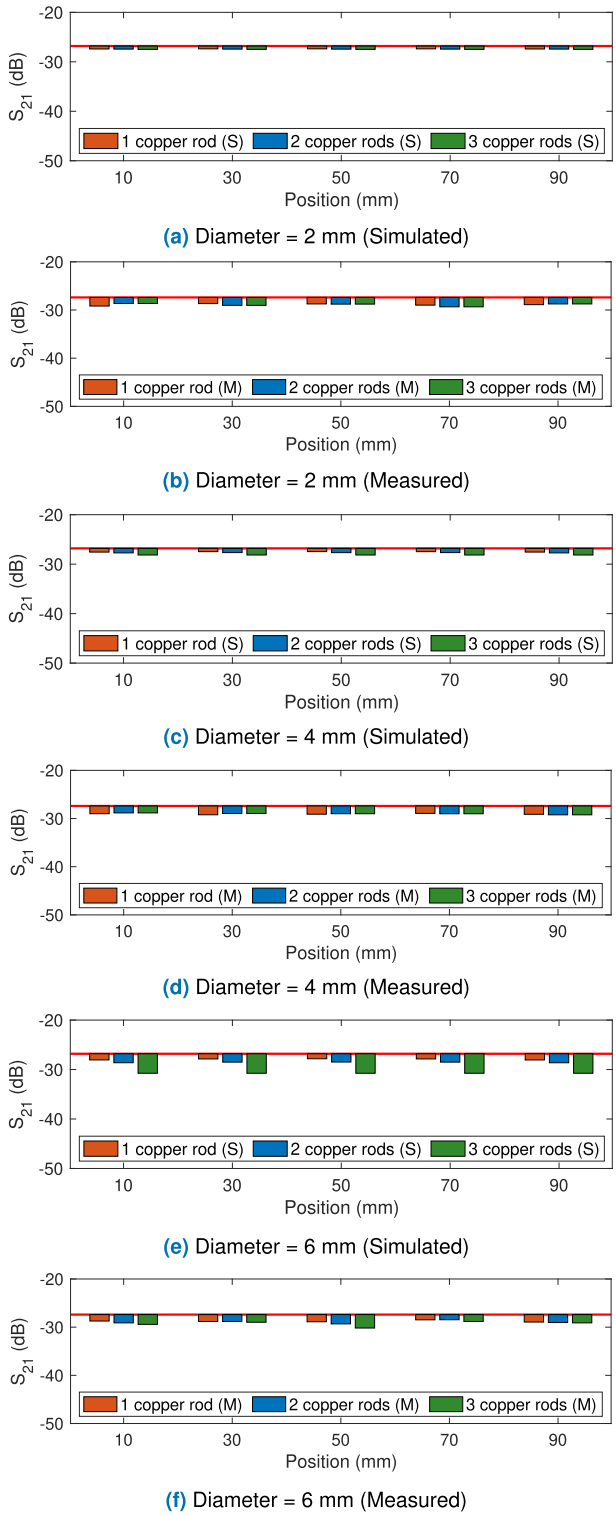

FIGURE 15. COPPER ROD: Simulated and measured S_{21} results for transverse-horizontal plane. (a, b) Diameter = 2 mm. (c, d) Diameter = 4 mm. (e, f) Diameter = 6 mm.

despite a larger diameter. Therefore, blood vessel formation and presence in such situation are less impactful towards signal coupling, explainable by the blood vessel orientation. The attribute allows E-field splitting using a coherent phase and subsequent signal recombination, as seen in literature [41].

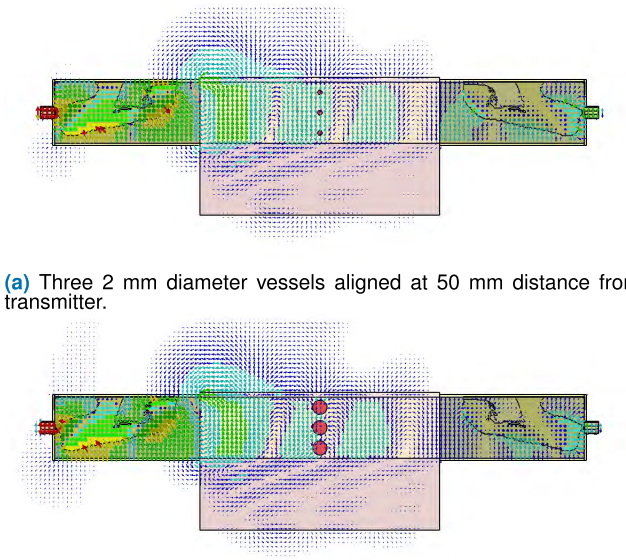

(a) Three 2 mm diameter vessels aligned at 50 mm distance from transmitter.

(b) Three 6 mm diameter vessels aligned at 50 mm distance from transmitter.

FIGURE 16. MUSCLE ROD: Electric field for three blood vessels in transverse-horizontal plane.

It can be concluded that dissimilarities of each configuration in their signal transmission performances are attributable to the position of the blood vessel. In the transverse-vertical plane, higher reflection is seen due to their reflector-based behavior, while blood vessels in the transverse-horizontal plane function as a splitter and recombiner. Meanwhile, the longitudinal plane is characterized by blood vessel that functions as a splitter, whereby there is no electric field recombination due to mismatched signal propagation.

The maximum signal loss for blood vessels configurations has been discussed. The bracketed value is the simulated outcomes, while non-bracketed values are the results obtained from the measurement. The longitudinal plane resulted in a maximum signal loss of 6.11 dB (4.56 dB) relative to the reference in case of the muscle rods when three 6 mm-sized vessels were positioned at $-T_{\text{fat/4}}$ (close to muscle). Meanwhile, the signal coupling revealed low-impact value of 2.94 dB (1.40 dB) when the vessels were positioned at $+T_{\text{fat/4}}$ (close to skin). In contrast, the maximum signal loss relative to the reference was recorded as 7.69 dB (6.14 dB) in case of the copper rod when three 6 mm-sized vessels were positioned at $+T_{\text{fat/4}}$ (close to skin). Meanwhile, the signal coupling revealed almost zero effect upon vessel placement at $-T_{\text{fat/4}}$ (close to muscle). Besides, the loss observed in the transverse-vertical plane displayed increments alongside increasing amount of vessel and vessel size. The signal loss of 2.79 dB (3.94 dB) in case of the copper rods and 3.42 dB (2.20 dB) in case of the muscle rods when three 6 mm-sized vessels were positioned in the channel. The signal loss with respect to reference in case of both cases are the same in all positions, which are vessel movement from 10 mm to 90 mm by 20 mm step. In transverse-horizontal plane, the maximum signal loss of 21.52 dB (20.94 dB) relative to the reference

TABLE 2. Comparison of simulated and measured transmission loss (S_{21}), average with respect to the fat channel [Average(Reference - S_{21})].

Vessel(s)	No. of Vessel(s)	Average S_{21} (dB) Measured (Simulated)					
		Longitudinal Plane		Transverse-vertical Plane		Transverse-horizontal Plane	
		Muscle	Copper	Muscle	Copper	Muscle	Copper
2 mm	1	1.17 (0.62)	2.39 (0.86)	0.83 (0.81)	1.51 (2.51)	1.79 (0.57)	1.50 (0.58)
	2	1.44 (0.67)	2.64 (0.91)	0.91 (0.88)	4.53 (3.35)	1.87 (0.65)	1.52 (0.70)
	3	2.47 (0.75)	2.90 (1.09)	1.05 (1.03)	9.12 (7.97)	1.92 (0.69)	1.52 (1.12)
	Average	1.70 (0.68)	2.64 (0.96)	2.12 (2.09)	5.44 (3.20)	1.86 (0.64)	1.51 (0.80)
4 mm	1	1.20 (0.93)	2.44 (1.10)	1.81 (1.79)	7.56 (3.21)	1.90 (0.68)	1.68 (0.67)
	2	1.68 (1.14)	2.86 (1.33)	2.07 (2.04)	9.47 (5.09)	2.15 (0.91)	1.61 (0.88)
	3	2.65 (1.46)	3.45 (1.70)	2.67 (2.66)	15.08 (11.70)	2.31 (1.10)	1.61 (1.74)
	Average	1.84 (1.17)	2.92 (1.37)	2.53 (2.50)	8.38 (5.19)	2.12 (0.90)	1.64 (1.08)
6 mm	1	2.26 (1.66)	2.62 (1.36)	3.71 (3.68)	7.25 (3.87)	2.17 (0.93)	1.38 (0.67)
	2	2.98 (2.11)	3.24 (1.90)	4.59 (4.58)	11.15 (7.13)	2.76 (1.53)	1.56 (1.34)
	3	4.50 (2.96)	4.15 (2.60)	5.13 (5.11)	17.13 (14.31)	3.42 (2.20)	1.91 (3.94)
	Average	3.25 (2.24)	3.33 (1.95)	2.95 (2.93)	13.77 (11.33)	2.79 (1.56)	1.62 (1.99)

in case of the copper rods when three 6 mm-sized vessels were positioned near to the transmitter or receiver. Contrary, the maximum signal loss of 5.59 dB (5.55 dB) in case of the muscle rods with the same condition were positioned in the center of the channel which is at 50 mm distance.

Additionally, Table 2 compares the simulated and measured transmission loss (S_{21}), which is enumerated in the form of average values relative to the fat channel across all places. The bracketed value is the simulated outcomes, while non-bracketed values are the results obtained from the measurement. In longitudinal plane, the average loss for 2 mm, 4 mm, and 6 mm diameter sizes of muscle rods was about 1.70 dB (0.68 dB), 1.84 dB (1.17 dB), and 3.25 dB (2.24 dB), respectively. These values were similar to the copper rod, which yielded 2.64 dB (0.96 dB), 2.92 dB (1.37 dB), and 3.33 dB (1.95 dB), respectively. Moreover, in transverse-vertical plane, muscle rod insertion from one to three vessels yielded the average loss of 2.12 dB (2.09 dB), 2.53 dB (2.50 dB), and 2.95 dB (2.93 dB), respectively, for all distances. Such losses were increased in case of larger-sized diameters and number of vessels. Similarly, the average loss was higher relative to the reference for all distances in case of copper rod insertion from one to three vessels, recording 5.44 dB (3.20 dB), 8.38 dB (5.19 dB), and 13.77 dB (11.33 dB), respectively. When copper rods were inserted as blood vessels, those positioned in the transverse-vertical plane attenuated and yielded the most signal coupling. The maximum loss in transverse-vertical plane was recorded to be 17.13 dB (14.31 dB) for three 6 mm-sized copper rods, thereby being the representative worst-case scenario compared to the longitudinal and transverse-horizontal planes. Finally, the average loss in transverse-horizontal plane for 2 mm, 4 mm, and 6 mm diameter sizes of 1.86 dB (0.64 dB), 2.12 dB (0.90 dB), and 2.79 dB (1.56 dB) in case of muscle rods and 1.51 dB (0.80 dB), 1.64 dB (1.08 dB), and 1.62 dB (1.99 dB) in a case of copper rods. The transverse-horizontal plane revealed the least effect in case of blood vessel presence, with a maximum average loss of 3.42 dB (2.20 dB) for muscle and 1.91 dB (3.94 dB) for copper rod. These were obtained from three 6 mm-sized vessels.

V. CONCLUSIONS

This work assessed the influence of blood vessels having varying orientations, diameter sizes, and positions towards the signal transmission for the fat-IBC application. The blood vessel orientation and its impact was evaluated using homogeneous three-layered ex-vivo porcine tissues across the three planes of transverse-vertical, transverse-horizontal, and longitudinal in the fat tissue. Simulations and experiments were both conducted using muscle and copper rods of different sizes. They were representative of the 2 mm, 4 mm, and 6 mm-sized blood vessels so as to efficiently evaluate the resulting impact towards signal transmission in fat-IBC. The following points are to be noted as per the simulated and measured results obtained (note that the bracketed value represents the simulated results, while the non-bracketed value represents the measured results):

- In the longitudinal plane, signal coupling shows more effect in case of muscle rod placement adjacent to the muscle layer ($-T_{\text{fat}/4}$), whereas similarly higher impact is seen in case of copper rods when positioned adjacent to the skin layer ($+T_{\text{fat}/4}$). This is due to disturbances of the peak electric field when being propagated, resulting in significant total average loss for both materials.
- Copper rod alignment in transverse-vertical direction along with propagation yields highly attenuated signal of up to 17.13 dB (14.31 dB) loss. It then vanished as the copper is highly conductive, upon number of vessel multiplied from one to three vessels, and in case of 6 mm-sized vessels.
- Muscle and copper rods positioned in the transverse-horizontal plane yield values with a difference

of 3.42 dB and 1.91 dB relative to the fat channel reference, as well as the least effect due to blood vessel presence.

The results obtained from measurements and simulations have both displayed excellent agreement and are well-supported via electric field visualization. Therefore, this confirms the reliability of the simulated outcomes obtained. Moreover, the higher conductivity of copper compared to blood vessels allowed this study to project the worst-case scenario of path loss. The transverse-vertical plane was found to display the most impact towards signal coupling and followed by the longitudinal plane, before the transverse-horizontal plane subsequently revealed the least impact with the blood vessel influence.

Such conclusion is indicative of the impact and influence posed by the size of blood vessel towards communication signal transmission. All outcomes obtained in this study collectively revealed the effect of blood vessel towards signal transmission and its potential function as the benchmark in the process of developing implant antennas for the fat-IBC technique. Therefore, this work will assist in the generation of implant communication methods in view of low power attributes and high-quality transmission. Future investigation should develop blood vessel modeling in the fat-IBC with blood velocity and body dynamics being considered as additional parameters.

REFERENCES

[1] J. Wang, Y. Nishikawa, and T. Shibata, "Analysis of on-body transmission mechanism and characteristic based on an electromagnetic field approach," *IEEE Trans. Microw. Theory Techn.*, vol. 57, no. 10, pp. 2464–2470, Oct. 2009.

[2] D. Werber, A. Schwentner, and E. M. Biebl, "Investigation of RF transmission properties of human tissues," *Adv. Radio Sci.*, vol. 4, pp. 357–360, Sep. 2006.

[3] J. Bae, H. Cho, K. Song, H. Lee, and H.-J. Yoo, "The signal transmission mechanism on the surface of human body for body channel communication," *IEEE Trans. Microw. Theory Techn.*, vol. 60, no. 3, pp. 582–593, Mar. 2012. doi: 10.1109/TMTT.2011.2178857.

[4] M. Swaminathan, F. S. Cabrera, J. S. Pujol, U. Muncuk, G. Schirner, and K. R. Chowdhury, "Multi-path model and sensitivity analysis for galvanic coupled intra-body communication through layered tissue," *IEEE Trans. Biomed. Circuits Syst.*, vol. 10, no. 2, pp. 339–351, Apr. 2016. doi: 10.1109/TBCAS.2015.2412548.

[5] M. S. Wegmueller, M. Oberle, N. Felber, N. Kuster, and W. Fichtner, "Galvanical coupling for data transmission through the human body," in *Proc. IEEE Instrum. Meas. Technol. Conf.*, Sorrento, Italy, Apr. 2006, pp. 1686–1689. doi: 10.1109/IMTC.2006.328197.

[6] Y. Song, Q. Hao, K. Zhang, M. Wang, Y. Chu, and B. Kang, "The simulation method of the galvanic coupling intrabody communication with different signal transmission paths," *IEEE Trans. Instrum. Meas.*, vol. 60, no. 4, pp. 1257–1266, Apr. 2011. doi: 10.1109/TIM.2010.2087870.

[7] M. A. Callejón, J. Reina-Tosina, D. Naranjo-Hernández, and L. M. Roa, "Measurement issues in galvanic intrabody communication: Influence of experimental setup," *IEEE Trans. Biomed. Eng.*, vol. 62, no. 11, pp. 2724–2732, Nov. 2015. doi: 10.1109/TBME.2015.2444916.

[8] M. D. Pereira, G. A. Alvarez-Botero, and F. R. de Sousa, "Characterization and modeling of the capacitive HBC channel," *IEEE Trans. Instrum. Meas.*, vol. 64, no. 10, pp. 2626–2635, Oct. 2015. doi: 10.1109/TIM.2015.2420391.

[9] J. Mao, H. Yang, and B. Zhao, "An investigation on ground electrodes of capacitive coupling human body communication," *IEEE Trans. Biomed. Circuits Syst.*, vol. 11, no. 4, pp. 910–919, Aug. 2017. doi: 10.1109/TBCAS.2017.2683532.

[10] Ž. Lučev, I. Krois, and M. Cifrek, "A capacitive intrabody communication channel from 100 kHz to 100 MHz," *IEEE Trans. Instrum. Meas.*, vol. 61, no. 12, pp. 3280–3289, Dec. 2012. doi: 10.1109/TIM.2012.2205491.

[11] G. E. Santagati, T. Melodia, L. Galluccio, and S. Palazzo, "Medium access control and rate adaptation for ultrasonic intrabody sensor networks," *IEEE/ACM Trans. Netw.*, vol. 23, no. 4, pp. 1121–1134, Aug. 2015.

[12] T. Bos, W. Jiang, J. D'hooge, M. Verhelst, and W. Dehaene, "Enabling ultrasound in-body communication: FIR channel models and QAM experiments," *IEEE Trans. Biomed. Circuits Syst.*, vol. 13, no. 1, pp. 135–144, Feb. 2019. doi: 10.1109/TBCAS.2018.2880878.

[13] R. D. Fernandes, J. N. Matos, and N. B. Carvalho, "Resonant electrical coupling: Circuit model and first experimental results," *IEEE Trans. Microw. Theory Techn.*, vol. 63, no. 9, pp. 2983–2990, Sep. 2015. doi: 10.1109/TMTT.2015.2458323.

[14] R. D. Fernandes, J. N. Matos, and N. B. Carvalho, "Constructive combination of resonant magnetic coupling and resonant electrical coupling," in *Proc. IEEE Wireless Power Transf. Conf. (WPTC)*, Boulder, CO, USA, May 2015, pp. 1–3. doi: 10.1109/WPT.2015.7140183.

[15] K. Zhao, Z. Ying, and S. He, "Intrabody communications between mobile device and wearable device at 26 MHz," *IEEE Antennas Wireless Propag. Lett.*, vol. 16, pp. 1875–1878, 2017. doi: 10.1109/LAWP.2016.2588524.

[16] N. B. Asan, D. Noreland, E. Hassan, S. R. M. Shah, A. Rydberg, T. J. Blokhuis, P.-O. Carlsson, T. Voigt, and R. Augustine, "Intra-body microwave communication through adipose tissue," *Healthcare Technol. Lett.*, vol. 4, no. 4, pp. 21–115, Aug. 2017.

[17] N. B. Asan, E. Hassan, J. Velander, S. M. Shah, D. Noreland, T. Blokhuis, E. Wadbro, M. Berggren, T. Voigt, and R. Augustine, "Characterization of the fat channel for intra-body communication at R-band frequencies," *Sensors*, vol. 18, no. 9, p. 2752, 2018. doi: 10.3390/s18092752.

[18] N. B. Asan, C. P. Penichet, S. R. M. Shah, D. Noreland, E. Hassan, A. Rydberg, T. J. Blokhuis, T. Voigt, and R. Augustine, "Data packet transmission through fat tissue for wireless intrabody networks," *IEEE J. Electromagn., RF Microw. Med. Biol.*, vol. 1, no. 2, pp. 43–51, Dec. 2017. doi: 10.1109/JERM.2017.2766561.

[19] M. H. Seyedi and D. T. H. Lai, "Effect of limb joints and limb movement on intrabody communications for body area network applications," *J. Med. Biol. Eng.*, vol. 34, no. 3, pp. 276–283, 2014.

[20] M. Seyedi, D. T. H. Lai, and M. Faulkner, "Limb joint effects on signal transmission in capacitive coupled intra-body communication systems," in *Proc. Annu. Int. Conf. IEEE Eng. Med. Biol. Soc.*, San Diego, CA, USA, Aug. 2012, pp. 6699–6702.

[21] X. M. Chen, S. H. Pun, J. F. Zhao, P. U. Mak, B. D. Liang, and M. I. Vai, "Effects of human limb gestures on galvanic coupling intra-body communication for advanced healthcare system," *Biomed. Eng. Online*, vol. 15, no. 1, p. 60, 2016. doi: 10.1186/s12938-016-0192-z.

[22] B. Kibret, M. Seyedi, D. T. H. Lai, and M. Faulkner, "An empirical comparison of limb joint effects on capacitive and galvanic coupled intra-body communications," in *Proc. IEEE 8th Int. Conf. Intell. Sensors, Sensor Netw. Inf. Process. (ISSNIP)*, Melbourne, VIC, Australia, Apr. 2013, pp. 318–323.

[23] S. Lin, H.-F. Zhang, Y.-M. Gao, M. Du, and M.-I. Vai, "The effects of muscle stress on signal transmission in the intra-body communication," in *Proc. IEEE Int. Conf. Consum. Electron.-China (ICCE-China)*, Guangzhou, China, Dec. 2016, pp. 1–3. doi: 10.1109/ICCE-China.2016.7849761.

[24] Z. Nie, J. Ma, H. Chen, and L. Wang, "Statistical characterization of the dynamic human body communication channel at 45 MHz," in *Proc. IEEE 28th Annu. Int. Conf. EMBC*, Jul. 2013, pp. 1206–1209.

[25] S. Lin, Y.-M. Gao, J. Cai, Ž. L. Vasic, M.-I. Vai, M. Du, M. Cifrek, and S.-H. Pun, "Biological evaluation of the effect of galvanic coupling intra-body communication on human skin fibroblast cells," *Wireless Commun. Mobile Comput.*, vol. 2017, Sep. 2017, Art. no. 8674035. [Online]. Available: https://doi.org/10.1155/2017/8674035.

[26] I. W. Ibrahim, A. H. A. Razak, A. Ahmad, M. K. M. Salleh, and R. N. Khir, "Body Mass Index (BMI) effect on galvanic coupling intra-body communication," *J. Telecommun., Electron. Comput. Eng.*, vol. 10, nos. 1–6, pp. 177–180, 2018.

[27] N. B. Asan, J. Velander, S. Redzwan, M. Perez, E. Hassan, T. J. Blokhuis, T. Voigt, and R. Augustine, "Effect of thickness inhomogeneity in fat tissue on in-body microwave propagation," in *Proc. IEEE Int. Microw. Biomed. Conf. (IMBioC)*, Philadelphia, PA, USA, Jun. 2018, pp. 136–138. doi: 10.1109/IMBIOC.2018.8428872.

[28] N. B. Asan, J. Velander, Y. Redzwan, R. Augustine, E. Hassan, D. Noreland, T. Voigt, and T. J. Blokhuis, "Reliability of the fat tissue channel for intra-body microwave communication," in *Proc. IEEE Conf. Antenna Meas. Appl. (CAMA)*, Tsukuba, Japan, Dec. 2017, pp. 310–313. doi: 10.1109/CAMA.2017.8273435.

[29] N. B. Asan, S. Redzwan, J. Velander, D. M. Perez, R. Augustine, E. Hassan, T. Voigt, and J. T. Blokhuis, "Effects of blood vessels on fat channel microwave communication," in *Proc. IEEE Conf. Antenna Meas. Appl. (CAMA)*, Västerås, Sweden, Sep. 2018, pp. 1–4. doi: 10.1109/CAMA.2018.8530527.

[30] X. Li, *Body Matched Antennas for Microwave Medical Applications*, vol. 72. Berlin, Germany: KIT Scientific Publishing, 2014.

[31] Society for Endocrinology. *You and Your Hormones*. Accessed: Mar. 1, 2019. [Online]. Available: http://www.yourhormones.info/glands/adipose-tissue/

[32] B. Koeppen and B. Stanton, *Berne and Levy Physiology*, 6th ed. Amsterdam, The Netherlands: Elsevier, 2008.

[33] Keysight Technologies. (2018). *Keysight N1501A Dielectric Probe Kit 10 MHz to 50 GHz*. Accessed: Mar. 5, 2019. [Online]. Available: https://literature.cdn.keysight.com/litweb/pdf/5992-0264EN.pdf

[34] S. Gabriel, R. W. Lau, and C. Gabriel, "The dielectric properties of biological tissues: II. Measurements in the frequency range 10 Hz to 20 GHz," *Phys. Med. Biol.*, vol. 41, no. 11, pp. 2251–2269, 1996.

[35] S. Gabriel, R. W. Lau, and C. Gabriel, "The dielectric properties of biological tissues: III. Parametric models for the dielectric spectrum of tissues," *Phys. Med. Biol.*, vol. 41, no. 11, pp. 2271–2293, 1996.

[36] C. Gabriel and A. Peyman, "Dielectric measurement: Error analysis and assessment of uncertainty," *Phys. Med. Biol.*, vol. 51, no. 23, pp. 6033–6046, 2006.

[37] M. A. Gibney, C. H. Arce, K. J. Byron, and L. J. Hirsch, "Skin and subcutaneous adipose layer thickness in adults with diabetes at sites used for insulin injections: Implications for needle length recommendations," *Current Med. Res. Opinion*, vol. 26, no. 6, pp. 1519–1530, 2010. doi: 10.1185/03007995.2010.481203.

[38] Keysight Technologies. (2018). *FieldFox Handheld Analyzers Data Sheet*. Accessed: Mar. 5, 2019. [Online]. Available: https://literature.cdn.keysight.com/litweb/pdf/5990-9783EN.pdf?id=2210837

[39] E. Hassan, D. Noreland, E. Wadbro, and M. Berggren, "Topology optimisation of wideband coaxial-to-waveguide transitions," *Sci. Rep.*, vol. 7, Mar. 2017, Art. no. 45110. doi: 10.1038/srep45110.

[40] D. J. Griffiths, "Reflection at a conducting surface," in *Introduction to Electrodynamics*, 3rd ed. Upper Saddle River, NJ, USA: Prentice-Hall, 1999, pp. 396–398.

[41] J. B. Marion and M. A. Heald, "Interference phenomena," in *Classical Electromagnetic Radiation*, 2nd ed. New York, NY, USA: Academic, 1965, p. 338.

NOOR BADARIAH ASAN (S'17) was born in Malaysia, in 1984. She received the B.Eng. degree in electronic engineering (telecommunication electronics) from Universiti Teknikal Malaysia Melaka, Malaysia, in 2008, and the M.Eng. degree in communication and computer from the National University of Malaysia, Selangor, Malaysia, in 2012. She is currently pursuing the Ph.D. degree with the Department of Engineering Sciences, Ångström Laboratory, Uppsala University, since 2015. In 2010, she joined the Department of Electronic and Computer Engineering, Universiti Teknikal Malaysia Melaka, as a Lecturer. She is working on characterizing and developing fat-intrabody microwave communication (Fat-IBC). Her current research interests include wireless sensor networks, material characterization, designing, optimizing, and characterizing biomedical sensor for intrabody area networks.

EMADELDEEN HASSAN received the B.Sc. and M.Sc. degrees in electronics and communication engineering from Menoufia University, Egypt, in 2001 and 2006, and the Licentiate and Ph.D. degrees in computational science and engineering from Umeå University, Umeå, Sweden, in 2013 and 2015, respectively. His research interests include numerical methods in EM, Antenna design optimization, EBG, defected ground structures, non-destructive evaluation and testing, optimization methods, and parallel programming.

MAURICIO DAVID PEREZ was born in Buenos Aires, Argentina, in 1980. He received the degree in electronics engineering from the National Technological University (UTN), Argentina, in 2007, and the Ph.D. degree in electrical engineering from the University of Bologna (UNIBO), Italy, in 2012. He was an Industrial Researcher in Italy, from 2012 to 2014, and as an Academic Teacher and Researcher with UTN, Argentina, from 2014 to 2017. He is currently a Teacher and also a Researcher with the Microwaves in Medical Engineering Group (MMG), Ångström Laboratories, Uppsala University (UU), Sweden. His research interests are on modeling and data-driven validation of microwave sensors for biomedical applications.

SYAIFUL REDZWAN MOHD SHAH (S'16) was born in Malaysia, in 1984. He received the B.Eng. degree in electronic engineering (telecommunication electronics) and the M.Sc. degree in communication and computer from Universiti Teknikal Malaysia Melaka, Durian Tunggal, Malaysia, in 2007 and 2010, respectively. He is currently pursuing the Ph.D. degree with the Department of Engineering Sciences, Uppsala University, Sweden. From 2011 to 2013, he was a Research Engineer with Huawei Technologies, Malaysia. He was with LG CNS Ltd., Malaysia, as a Senior Research Engineer, from 2013 to 2015. His research interests include designing BMD sensors, microwave material characterization, noninvasive diagnostics, and biomedical sensors.

JACOB VELANDER was born in Uppsala, Sweden, in 1981. He received the B.Sc. degree in electrical engineering and the M.Sc. degree in technology from the Department of Engineering Sciences, Uppsala University, Sweden, in 2015 and 2016, respectively. He is currently pursuing the Ph.D. degree with Ångström Laboratory, Microwave Group, Solid State Electronics, Department of Engineering, Uppsala University, Sweden. He has worked as a Project Assistant for low-frequency simulations with the Department of Engineering Sciences, Solid State Electronics, Uppsala University. In parallel, he is involved in two projects by name, Comfort, Complex fracture orthopedic and BDAS, and Bone Density Analysis System, both for monitoring bone mineral density. His current works include artificial models (phantoms) fabrication for craniosynostosis, hip fracture, and skin burn. He is also involved in BMD sensor development, CST simulations, and body tissue characterizations in ex-vivo and in-vivo context.

TACO J. BLOKHUIS received the degree in medicine in Amsterdam, The Netherlands, in 1996, and the Ph.D. degree, in 2001. After finishing his training as a Trauma Surgeon, he has been working in university medical centers throughout The Netherlands. In 2014, he was appointed as an Associate Professor with the University of Utrecht, The Netherlands. He is currently with the Maastricht University Medical Center, The Netherlands. Besides his clinical tasks, his focus is on basic (preclinical) research.

THIEMO VOIGT (M'14) received the Ph.D. degree from Uppsala University, Sweden, in 2002. He is currently a Professor of computer science with the Department of Information Technology, Uppsala University. He also leads the Networked Embedded Systems Group, RISE SICS. His current research focuses on system software for embedded networked devices and the Internet of Things. His work has been cited more than 12 000 times. He is a member of the editorial board for the IEEE INTERNET OF THINGS and the *ACM Transactions on Sensor Networks* (TOSN).

ROBIN AUGUSTINE (M'14) received the master's degree in electronics science from Mahatma Gandhi University, Kottayam, India, in 2003, and the master's degree in electronics from the Cochin University of Science and Technology, Cochin, India, in 2005, and the Ph.D. degree in electronics and optronics systems from the Université de Paris Est Marne La Vallée, France, in 2009. His current research interests include the design of wearable antennas, BMD sensors, dielectric characterization, intrabody area networks, bioelectromagnetism, noninvasive diagnostics, and biological healing effects of RF in *in vitro* and *in vivo* systems. He completed his postdoctoral training at the University of Rennes 1, IETR, from 2009 to 2011. Since 2011, he has been a Senior Researcher with Uppsala University, Sweden. In 2016, he was appointed Docent (Associate Professor) in microwave technology with Uppsala University. He is the Swedish PI of the Eureka Eurostars Project COMFORT and Indo-Swedish Vinnova-DST funded project BDAS. He was granted the Swedish Research Council (VR) funding for his project Osteodiagnosis. He is also the WP leader of the H2020 Project SINTEC and the Co-PI of the framework project LifeSec from the Swedish Strategic Foundation (SSF). He is responsible for the lead technical development in the Eurostars Project SenseBurn. He is leading the microwaves at the Medical Engineering Group (MMG), Solid State Electronics Division, Uppsala University. Since 2019, he has been a Visiting Professor with the Beijing Institute of Nanoenergy and Nanosystems (BINN), Beijing. He is the author or coauthor of more than 110 publications, including journals and conferences in the field of sensors, microwave antennas, bioelectromagnetics, and material characterization. He received the UGCRFSMS Fellowship for meritorious students from the Indian Government and the EGIDE Eiffel Grant for excellence from the French Research Ministry, in 2006 and 2008, respectively. He is a member of the editorial board for the *IET Electronics Letters* and the *Medical Research and Innovation Journal*.